

# Anisotropy of electronic stopping power in graphite

Jessica Halliday<sup>1</sup> and Emilio Artacho<sup>1,2,3</sup>

<sup>1</sup>*Theory of Condensed Matter, Cavendish Laboratory, University of Cambridge, J. J. Thomson Ave, Cambridge CB3 0HE, United Kingdom*

<sup>2</sup>*CIC Nanogune and DIPIC, Tolosa Hiribidea 76, 20018 San Sebastian, Spain*

<sup>3</sup>*Ikerbasque, Basque Foundation for Science, 48011 Bilbao, Spain*

(Dated: May 20, 2019)

The rate of energy transfer from ion projectiles onto the electrons of a solid target is hard to determine experimentally in the velocity regime between the adiabatic limit and the Bragg peak. First-principles simulations have lately offered relevant new insights and quantitative information for prototypical homogeneous materials. Here we study the influence of structural anisotropy on electronic stopping power with time-dependent density functional theory simulations of a hydrogen projectile in graphite. The projectile travelled at a range of angles and impact parameters for velocities between 0.1 and 1.4 a.u., and the electronic stopping power was calculated for each simulation. After validation with average experimental data, the anisotropic crystal structure was found to have a strong influence on the stopping power, with a difference between simulations parallel and perpendicular to the graphite plane of up to 25%, more anisotropic than expected based on previous work. The velocity dependence at low velocity displays clear linear behaviour in general, except for projectiles travelling perpendicular to graphitic layers, for which a threshold-like behaviour is obtained. For projectiles travelling along graphitic planes metallic behaviour is observed with a change of slope when the projectile velocity reaches the Fermi velocity of the electrons.

## I. INTRODUCTION

Stopping power is the rate of energy loss along the path of a charged particle as it passes through matter. Stopping power is of interest in a wide range of areas, from nuclear power generation to medical applications<sup>1,2</sup>. Two mechanisms of energy loss are involved: nuclear stopping, due to the interaction of the projectile with the nuclei of the target, and electronic stopping, from the interaction of the projectile with the electrons of the target. This work focusses on the electronic stopping power ( $S_e$ ) which dominates at high projectile velocities. Both theoretical and experimental work on electronic stopping has generally calculated a single average value of  $S_e$ , ignoring the anisotropy of the structure<sup>3-5</sup>. Anisotropy in crystal structure has a significant influence on many properties of materials<sup>6</sup>, however there is little work on the relationship between anisotropy and electronic stopping power<sup>7,8</sup>.

Experimentally  $S_e$  is difficult to measure directly, particularly at low velocities where nuclear stopping is also significant; simulations, however, allow  $S_e$  to be directly accessed. Echenique *et al.*<sup>9,10</sup> used density functional theory to calculate electronic stopping power in jellium, capturing non-linear effects and replicating experimental results not captured in linear-response theory calculations<sup>11,12</sup>, also giving rise to derived simulations, including the use of first principles techniques for the indirect calculation of  $S_e$  (for reviews see<sup>13,14</sup>). Direct, real-time simulations of the electronic stopping process have also been performed during the last decade using a time-dependent tight binding description of the electronic structure and dynamics, coupled to nuclear dynamics within an Ehrenfest approach<sup>15,16</sup>, providing interesting and rich qualitative insights, especially powerful

given the large system size and long time scale affordable with an empirical tight-binding scheme. In recent years time-dependent density functional theory (TDDFT) has been used to investigate stopping power from first principles in bulk materials of different kinds (metals, semiconductors, insulators)<sup>17-26</sup>. First principles simulation of electronic stopping has successfully reproduced many experimental features not captured by other theoretical or simulation methods.

A prototypical material with a highly anisotropic layered structure is graphite, composed of weakly bonded layers of strongly hexagonally bonded carbon atoms, resulting in a high degree of inhomogeneity in many properties<sup>27</sup>. A major use of graphite is as a moderator in the nuclear power industry, to absorb and slow down the neutrons generated by the nuclear fission processes, in order to control the rate of fission within a nuclear reactor. The stopping power of graphite is thus of intrinsic interest, in addition to its position as a simple and strongly anisotropic material, and was therefore chosen as the target material in this work. The velocity dependence of  $S_e$  is addressed in the work, with an emphasis on its variation with trajectory.

A previous work on anisotropy of stopping power in graphite is a theoretical study by Crawford<sup>7</sup>, using linear response theory based on the Cazaux model<sup>28</sup> for the optical constants of graphite parallel and perpendicular to the graphitic layers. Crawford's work calculated, for higher energy projectiles, a similar relationship between the incident angle of the projectile and the  $S_e$  as this work. They found a small anisotropy of  $S_e$ , with a variability of around 10% for projectile velocities between 2 and 20 a.u.. More recent work by Shukri, Bruneval and Reining<sup>8</sup> used linear response TDDFT to predict the random electronic stopping power in various materials. They

found a similar small anisotropy of up to 3% between the  $S_e$  along the in-plane and out-of-plane axes of graphite, for velocities between 0 and 4 a.u.. Previous experimental work by Yagi *et al.*<sup>29</sup> was unable to direct projectiles between the graphitic layers, illustrating the usefulness of simulations to investigate the structural anisotropy of  $S_e$ .

## II. METHOD

### A. Simulation details

Simulations were carried out using the real-time TDDFT implementation<sup>30,31</sup> of the SIESTA method<sup>32,33</sup>. The Kohn-Sham orbitals are expanded in a finite basis set of numerical atomic orbitals, with the valence electrons of graphite and the projectile represented by a double- $\zeta$  polarised basis set. The core electrons have been replaced by norm-conserving pseudopotentials using the Troullier-Martins scheme<sup>34,35</sup>. Core electrons are known not to interact in stopping processes at low velocities<sup>8,36</sup>. The details of both the basis set and the pseudopotentials are specified in the Appendix. The local density approximation (LDA) was used for the exchange-correlation functional evaluation using the Ceperley-Alder results for the homogeneous electron liquid<sup>37</sup>, in the parameterisation of Perdew and Zunger<sup>38</sup>, considering adiabatic time dependence of the exchange-correlation functional.

The ground state of the system is calculated with the projectile stationary at its initial position in the graphite box. Subsequent TDDFT simulations evolve the electronic wavefunctions according to the time-dependent Kohn-Sham equation<sup>39,40</sup> as the projectile moves at a constant velocity through the box. The forces on all atoms are held as zero throughout the time-dependent simulation, so that energy transfer only takes place through inelastic scattering to the system electrons. This prevents any contribution from nuclear stopping and enables the  $S_e$  to be directly calculated at a single velocity for each simulation. The electronic stopping is the average gradient of the total energy of the electronic system as a function of the path length of the projectile<sup>25</sup>. The error bars in the  $S_e$  presented in the figures refer to uncertainty in fitting to the slope.

Projectiles moved the full length of the simulation cell, 13.4 Å. Simulations were carried out using projectiles with velocities between 0.1 and 1.4 a.u.<sup>41</sup>. The time-dependent Kohn-Sham equations were integrated using a Crank-Nicholson integrator as in Ref. 30 adapted to the changing basis and Hilbert space by using a Löwdin transformation as proposed by Sankey and Tomkoff<sup>42</sup> and analysed in Ref. 43. See the Appendix for further details of convergence testing.

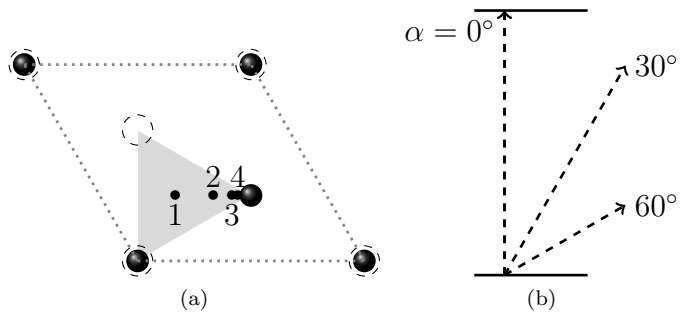


FIG. 1. (a) Graphite unit cell showing the projectile initial positions 1-4 and (b) trajectories for simulations of projectiles moving out of the plane of graphitic layers. The shaded triangle in (a) is the region of crystallographically unique positions.  $\alpha$  is the angle of the trajectory from the graphite  $c$  axis, with  $\alpha = 0^\circ$  perpendicular to the graphitic planes.

### B. Simulation trajectories

Simulations were run with a combination of the following parameters: the velocity of the projectile varied between 0.1 and 1.4 a.u., and the initial angle of the projectile relative to the  $c$  axis of the graphite,  $\alpha$ , varied between  $0^\circ$  and  $90^\circ$  as shown in Figure 1b. For simulations of projectiles moving parallel to the graphitic layers, the projectiles moved at an angle  $\beta$  relative to the  $a$  axis, at  $0^\circ$  and  $30^\circ$ , with checks at  $60^\circ$  and  $90^\circ$  as shown in Figure 2a, and moving at distances of  $\frac{1}{2}$ ,  $\frac{1}{4}$ ,  $\frac{1}{8}$  and  $\frac{1}{16}$  of the spacing between the layers from the closest graphitic layer, as shown in Figure 2b.

Concerning the charge state of the projectile, previous TDDFT work on electronic stopping has been carried out with both ions and atoms<sup>17,21,22,25</sup>. In this type of simulation, the use of a proton or a H atom only changes the simulation by one electron in the supercell (out of 129). The extent to which the proton drags an electron

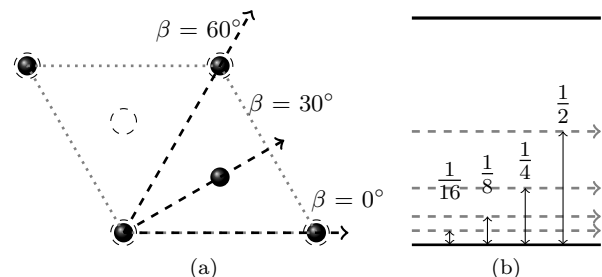


FIG. 2. (a) Graphite unit cell showing the projectile trajectories for simulations of projectiles moving parallel to the graphitic layers ( $\alpha = 90^\circ$ ).  $\beta$  is the angle of the trajectory from the  $a$  axis of the unit cell.  $\beta = 0^\circ$  and  $60^\circ$  are crystallographically equivalent. (b) Distance of projectile trajectories from the graphitic planes.

in its wake is defined dynamically, and the established stationary state is independent of the initial charge state of the projectile. After the initial transient, essentially the same state evolves regardless of whether it was initially  $H^+$  or  $H$ , in comparison with other methods in which the charge state is defined by hand<sup>13</sup>. The calculations presented here had 129 electrons in the simulation box, thereby defining an overall neutral system. The calculations were spin-polarised due to the odd number of electrons in the system.

### III. RESULTS AND DISCUSSION

#### A. Validation

In order to validate the simulations, the results are compared in Figure 3 with experimental data from work by Käferböck *et al.*<sup>3</sup>. In the velocity range covered by the experimental data, electronic stopping dominates the overall stopping power, so the simulations of electronic stopping are directly comparable to the Käferböck data. The Rutherford backscattering experiment used protons with an energy of between 20 and 80 keV/nucleon, corresponding to projectile velocities between 1 and 1.7 a.u., with a target of highly ordered pyrolytic graphite, although they did not provide angle resolution for the measured  $S_e$ . They consider ion trajectories in all directions.

In Figure 3, the agreement between experiment and theory is clear, with the experimental observations lying within the simulation range defined by different trajectories. The experimental stopping power is closest to that of the higher angle simulations,  $\alpha = 60^\circ - 75^\circ$ . As channelling directions were avoided in the experiments, it is likely that trajectories close to  $\alpha = 90^\circ$  contribute little to the experimental averaging. See a similar consideration in the work of Schleife *et al.*<sup>24</sup> for a proton moving in aluminium. In order to compare the simulations to the experimental data in more detail, a model of the distribution of projectile trajectories would be needed to calculate an average  $S_e$  for a particular velocity, which involves non-trivial assumptions on the actual trajectories in experimental settings.  $S_e$  gradually diminishes toward the minimum at  $\alpha = 90^\circ$ , starting at around  $\alpha = 50 - 60^\circ$  where a slight maximum appears, especially at low velocities.

#### B. Dependence on $\alpha$

Figure 3 shows the expected overall linear dependence of  $S_e$  in the displayed velocity range, with a slow downward bending as velocity increases towards the  $S_e$  maximum related to the Bragg peak, which in graphite is at  $\sim 1.9$  a.u.<sup>44</sup>. The curve for  $\alpha = 90^\circ$  is clearly different, however, corresponding to trajectories parallel to graphitic planes. As Figure 4 shows more clearly, the electronic stopping power decreases significantly at all

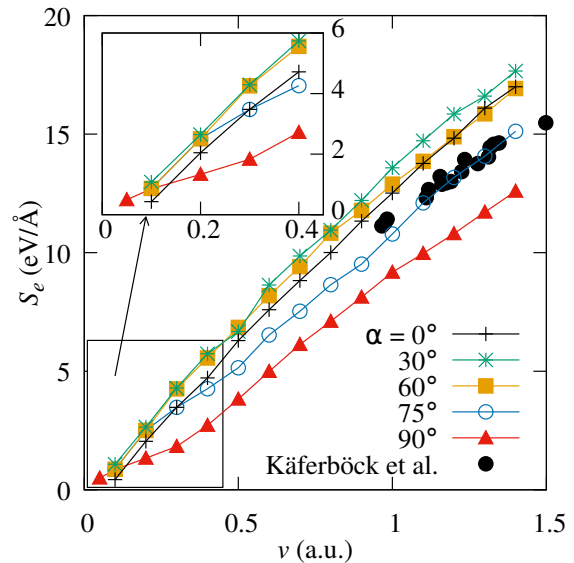


FIG. 3. Electronic stopping power for a proton shooting through graphite at different angles relative to the graphite  $c$  axis.  $\bullet$  depicts the experimental data from the work by Käferböck *et al.*<sup>3</sup>. The uncertainty in each data point is  $\pm 0.6$  eV/Å.

velocities between  $\alpha = 60^\circ$  and  $\alpha = 90^\circ$ . The data for  $\alpha = 90^\circ$  correspond to the projectile moving midway between two planes of atoms along  $\beta = 0^\circ$  (See Figures 1a and 2a).

Figure 4 also includes the linear-response results of Crawford<sup>7</sup> for comparison. The lowest velocity considered in that work is  $v = 2.0$  a.u., higher than those obtained in this work, which accounts for the higher overall  $S_e$ . They also show a smaller angle dependence, of approximately 10% between a projectile moving along  $\alpha = 0^\circ$  and  $90^\circ$  at 2 a.u., with smaller differences at higher projectile velocities; significantly lower than the equivalent difference for  $v = 1.0$  a.u. in our case. This is consistent with a further insensitivity with direction at high velocities<sup>7</sup>. Figure 9 of Shukri, Bruneval and Reining's paper<sup>8</sup> also shows a small difference of up to 3% in  $S_e$  between calculations with a projectile moving along  $\alpha = 0^\circ$  and  $90^\circ$  in graphite at velocities between 0 and 4 a.u.. As discussed below, that work calculated the random electronic stopping power, which is averaged over all impact parameters, and so is not directly equivalent to the results in this paper.

##### 1. Correlation of $S_e$ and electron density

Figure 4b shows the average electron density along a given trajectory versus  $\alpha$  for comparison with  $S_e(\alpha)$ . The relationship between the electron density and  $S_e$  is especially clear for the low velocities, with both  $S_e$  and electron density increasing from  $\alpha = 0^\circ$  to  $30^\circ$ , and the lowest

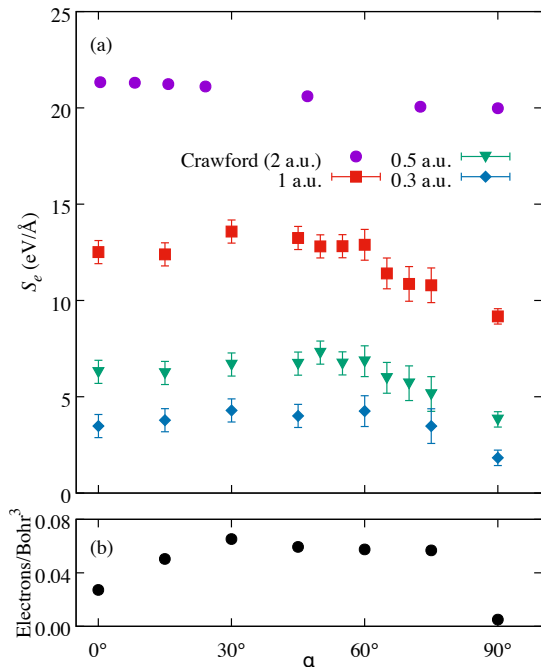


FIG. 4. (a) Electronic stopping power of a hydrogen atom in graphite moving at angle  $\alpha$  from the graphite  $c$  axis at a velocity of 0.3, 0.5 and 1.0 a.u.. The data for  $90^\circ$  were calculated from simulations with the projectile moving midway between two planes of atoms along  $\beta = 0^\circ$  (See Figures 1a and 2a). The error bars are due to the uncertainty in fitting to the slope of the energy plot. (b) Average electron density along the trajectory of the projectile for different  $\alpha$  values.

$S_e$  at  $90^\circ$  corresponding to the lowest electron density.

Under the scattering theory formalism developed by Echenique and others for jellium<sup>10,45–47</sup>, the target electron density is space independent, a number  $n$ , and the stopping power is a function  $S_e(v, n)$ , which starts at zero for  $n = 0$  and increases with higher density. This results has been generalised to non-homogeneous electron systems, with the observation that the stopping power is larger when the projectiles traverse regions of higher density. This has been seen in previous work in various materials<sup>25,45–47</sup>, and is used as a basic assumption in different contexts, as a local-density stopping approximation<sup>47</sup>. The results of the simulations presented here are consistent with this; between the graphitic layers the electron density is much lower than across the layers, and the higher the angle of the projectile relative to the  $c$  axis the more time it spends in the lower electron density region between the layers. As a result the projectile interacts less with the electrons of the target and so the  $S_e$  is lower, as seen in Figure 4, obtaining the minimum  $S_e$  for  $\alpha = 90^\circ$  and the projectile moving midway between the planes, that is, the trajectory furthest from the carbon atoms and thus with the lowest electron density. It must be noted, however, that although the correlation is clear, it is not strict, as can

be observed for  $\alpha = 75^\circ$ .

## 2. Channelling

The main channelling direction in graphite is along the  $c$  axis ( $\alpha = 0^\circ$ ), but the effect on  $S_e$  is limited. Only a small depression can be observed for  $S_e$  for  $\alpha = 0^\circ$  as compared with  $15^\circ$  at low velocity. In Figure 4 it is visible for  $v = 0.3 - 0.5$  a.u., but it is clearly a much smaller effect than the one for  $\alpha = 90^\circ$  (parallel to graphitic layers) even if using perfect channelling trajectories, as trajectory 1 in Figure 1a. These results are consistent with the previous discussion, since the average density along that path does not reduce as much as for those parallel to and midway between graphitic planes.

Channelling in a crystal occurs when a projectile arrives into a channel in a trajectory within a small angle from the channel in a major crystal direction, and then moves along it undergoing small angle scattering, thereby moving along the channel. As a result of the lack of nuclear collisions with the target material (beyond the small deflections implied by the channelling itself) and thereby reduced total energy loss of the projectile, the projectile travels further compared with a random direction in the crystal<sup>48</sup>.  $S_e$  would also be expected to be lower along a channelling direction, due to the lower average electron density in a channel; Schleife, Kanai and Correa<sup>24</sup> carried out TDDFT simulations of H in Al, comparing projectiles moving along channels with off-channelling directions, and found lower  $S_e$  for a projectile moving along a channelling direction than along a random non-channelling direction. Channelling in graphite has only been experimentally observed when the projectile is moving along the  $c$  axis of graphite, perpendicular to the graphitic layers<sup>49–51</sup>. That work used polycrystalline highly oriented pyrolytic graphite (HOPG), containing grain boundaries perpendicular to the graphitic layers, which would disrupt channelling between the layers. In HOPG, the basal planes are closely aligned, but alignment along the other axes is difficult to achieve. In theory, channelling would also be expected for a projectile travelling parallel to the graphitic layers, and the projectiles moving along  $\alpha = 90^\circ$  do show significantly lower  $S_e$ .

## 3. Low velocity

The behaviour of  $S_e$  in the low velocity end of Figure 3 is remarkable. On the one hand, the simulations with the projectile moving at angles other than  $90^\circ$  to the  $c$  axis appear to show a threshold velocity of 0.02-0.06 eV below which, extrapolating the calculated data,  $S_e$  appears to be either zero or very small on that scale. This is consistent with behaviour seen in insulators<sup>25</sup> where the band gap results in a velocity threshold for  $S_e$ . Graphite is effectively a semiconductor in the direction perpendicular

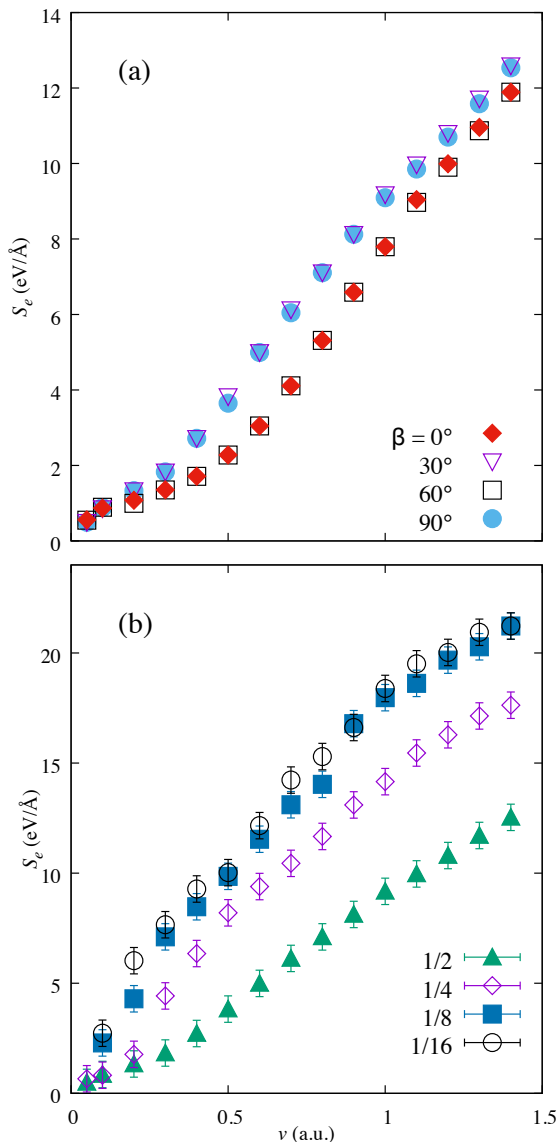


FIG. 5. (a) shows the electronic stopping power for a projectile moving parallel to the graphitic layers at angles  $\beta$  from the  $a$  axis of graphite, midway between the graphitic layers. (b) compares the electronic stopping power for a proton moving at different distances from the graphitic layers as a fraction of the interplanar distance (Figure 2a). The electronic stopping power increases the closer the path of the projectile is to a graphitic layer, likely due to the higher electron density closer to the planes.

to the graphitic layers, and, in that sense, this behaviour would appear to be consistent with what is expected, at least qualitatively. In contrast, the obtained  $S_e$  shown in Figure 3 for  $\alpha = 90^\circ$ , corresponding to a projectile moving midway between the graphitic layers, displays a very different behaviour, with no apparent threshold but rather  $S_e \propto v$ , but with a clear change of slope at  $v \sim 0.3$  a.u. displayed by the lowest  $S_e(v)$  graph in Figure 3.

### C. Protons travelling between graphitic planes

Figure 5 shows the behaviour for trajectories parallel to the graphitic planes in more detail, with the  $S_e(v)$  dependence for different orientations (Fig. 5a) and different impact parameters (proximity of the trajectory to the closest plane, Fig. 5b). Starting with Figure 5a, as discussed above, the  $S_e$  is much lower at all velocities and all angles where the projectile is travelling parallel to the graphitic layers, as a result of the lower electron density between the layers. Due to the hexagonal symmetry of graphite, the trajectories  $\beta = 0^\circ$  and  $\beta = 60^\circ$  are crystallographically identical.  $S_e(\beta)$  should therefore be periodic with a period of  $60^\circ$ . It is expected to be symmetric around  $0^\circ$  and  $30^\circ$ , the values of  $S_e$  for those  $\beta$ 's representing likely bounds for  $S_e(\beta)$ . Figure 5a shows  $S_e$  at  $0$  and  $30^\circ$  as a function of velocity. The periodicity has been checked with the inclusion of results for  $\beta = 60^\circ$  and  $90^\circ$ .

Figure 5(a) shows that the change of slope remains apparent for trajectories equidistant from two graphitic planes, irrespective of the  $\beta$  angle, although for  $\beta = 0^\circ$  it happens at a slightly larger value of  $v$  ( $v_K \sim 0.4$  a.u.) than for  $\beta = 30^\circ$  ( $v_M \sim 0.3$  a.u.). The former corresponds to the direction of the K-point in reciprocal space, while the latter to the M-point direction. Both values are close to the Fermi velocity of electrons around the Dirac cone ( $v_F = 0.37$  a.u.), indicating that the change of slope is due to the onset of intra-cone electron-hole transitions contributing to the stopping. We base this observation on the fact that the electron-hole excitations generated by the moving projectile should respect the relation<sup>25</sup>

$$\mathbf{v} \cdot \Delta \mathbf{k} = \Delta \epsilon$$

being  $\Delta \mathbf{k}$  and  $\Delta \epsilon$  the momentum and energy change of the electron, respectively, in the excitation, and  $\mathbf{v}$  the projectile's velocity. For  $v < v_F$ , excitations can only be connecting across cones, while for  $v \geq v_F$  the intra-cone channel is open.

A similar increase in the  $S_e$  gradient at velocities between 0.3 and 0.5 a.u. has been seen in experiments for various systems: protons in Au<sup>52,53</sup>, He in Al<sup>54</sup>, and protons and He in Cu<sup>55</sup>, to name a few. The change in gradient for the Cu and Au experiments is suggested to be a result of interactions with the target's  $3d$  and  $5d$  electrons in Cu and Au respectively at higher projectile velocities, where a minimum energy transfer is required for the excitation of  $d$  electrons in both metals<sup>52</sup>. For He in Al, the slope change is thought to be due to charge-exchange processes between the target atoms and projectile<sup>54</sup>. This again suggests that the increase in gradient is due to additional energy loss mechanisms becoming accessible beyond a certain velocity, and which, in this case would correspond to the mentioned intra-cone transitions, meaning electron-hole-pair formation within the same band and small momentum transfer within the Brillouin zone, as the velocity approaches the Fermi velocity of the host.

### 1. Impact parameter dependence

The impact parameter dependence is shown in Figure 5b. It compares the  $S_e$  for a projectile moving midway between the graphitic layers, and at positions  $\frac{1}{4}$ ,  $\frac{1}{8}$  and  $\frac{1}{16}$  of the interplanar distance from a graphitic layer, as shown in Fig. 2(b). The  $S_e$  is higher at all velocities above 0.1 a.u. for the simulations closer to the graphite atoms, corresponding to the higher electron density closer to the graphitic layer. The gradient of the  $S_e$  plot changes as the velocity increases, with a linear region between 0.5 and 1 a.u., and a slight decrease in gradient at higher velocities for both paths as the  $S_e$  approaches a maximum. When the trajectories get closer to either atomic plane (Fig. 5b)  $S_e$  significantly increases as compared to the mid-plane trajectory, and the clean two-slope structure of Figure 5(a) is lost, which should be attributed to scattering amplitude effects.

Trajectories perpendicular to the graphitic planes do not display significant impact-parameter dependence, however, unlike what is seen for trajectories parallel to the planes.  $S_e$  increased only by 0.68 eV/Å when changing from trajectory 1 in Figure 1a to trajectory 4 at  $v = 0.5$  a.u..

The results of Shukri, Bruneval and Reining<sup>8</sup> investigated random electronic stopping power, defined as the  $S_e$  averaged over all impact parameters. For the in-plane simulations, this is equivalent to averaging  $S_e$  for all the trajectories at different distances from the graphitic layers. As Figure 5 shows, there is a significant increase in  $S_e$  as the trajectory gets closer to a graphitic layer. The 3% difference between in-plane and out-of-plane simulations in  $S_e$  seen by Shukri *et al.*<sup>8</sup> is therefore consistent with the results in this work.

## IV. CONCLUSIONS

Simulations of a hydrogen projectile travelling through graphite successfully reproduced experimental results, and provided new insights into the effect of the anisotropy of the graphite structure on electronic stopping power. The electronic stopping power is dependent on the direction of the projectile both relative to the graphitic layer normal and parallel to the layers. Although a clear correlation is found between the local electron density traversed by the trajectory in general, at low velocity  $S_e$  displays varied behaviours depending on the direction and impact parameter. For channelling between planes and low density, a linear  $S_e$  is observed, consistent with (semi)metallic electron conduction, but which changes slope when the projectile velocity reaches the Fermi velocity of the target. For trajectories with dominant component perpendicular to the graphitic plane, a threshold is observed at  $v \sim 0.05$  a.u., consistent with poor electron conduction between planes.

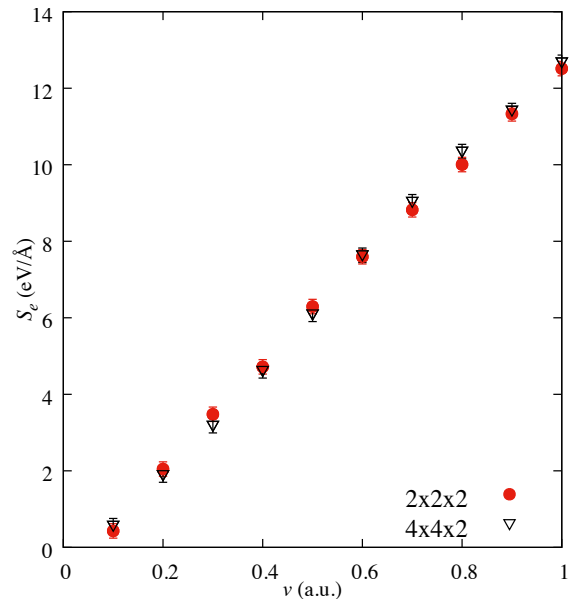


FIG. 6. Comparison of electronic stopping power in graphite with a hydrogen projectile travelling at 0.1 to 1 a.u. with supercell sizes of  $2 \times 2 \times 2$  and  $4 \times 4 \times 2$  primitive unit cells. In these simulations the projectile moved perpendicular to the graphitic planes along the shortest supercell dimension, through the center of a channel.

## ACKNOWLEDGMENTS

The authors would like to thank Pere Alemany for useful discussions on this work. Jessica Halliday would like to thank Rafi Ullah for his technical help in the initial stages of this work. This work was performed using resources provided by the Cambridge Service for Data Driven Discovery (CSD3) operated by the University of Cambridge Research Computing Service (<http://www.csd3.cam.ac.uk/>), provided by Dell EMC and Intel using Tier-2 funding from the Engineering and Physical Sciences Research Council (capital grant EP/P020259/1), and DiRAC funding from the Science and Technology Facilities Council ([www.dirac.ac.uk](http://www.dirac.ac.uk)). Jessica Halliday would like to acknowledge the EPSRC Centre for Doctoral Training in Computational Methods for Materials Science for funding under grant number EP/L015552/1.

## APPENDIX

This section describes the testing carried out to generate the initial simulation parameters. The pseudopotentials of C and H were generated using the scheme of Troullier and Martins<sup>35</sup> and the corresponding parameters are shown in Table I.

TABLE I. Pseudopotential radii for each angular-momentum channel of C and H. Lengths are in Bohr.

Species	$s$	$p$	$d$	$f$
C ( $2s^2 2p^2$ )	1.49	1.50	1.56	1.56
H ( $1s^2$ )	1.25	1.25	1.25	1.25

Table II gives the parameters needed for the generation of the basis set used in this work, following the procedures described in Ref. 56. The polarisation orbitals were generated by applying an electric field to the orbital according to the procedure implemented in SIESTA and described in Ref. 32.

TABLE II. Cutoff radii  $r(\zeta_1)$  and  $r(\zeta_2)$  in Bohr of the first and second  $\zeta$  functions of C and H.

Species	$n$	$l$	$r(\zeta_1)$	$r(\zeta_2)$
C	2	0	4.192	3.432
	2	1	4.870	3.475
H	1	0	4.828	3.855

A periodic supercell of  $2 \times 2 \times 2$  graphite unit cells was used, containing 32 C atoms and a single H atom, with lattice parameters of  $a = 2.461 \text{ \AA}$ ,  $c = 6.573 \text{ \AA}$ . A number of supercell sizes were tested to confirm that the supercell used was sufficiently large to give good quality results. Figure 6 compares the electronic stopping power for a projectile moving perpendicular to the graphitic layers in  $2 \times 2 \times 2$  and a  $4 \times 4 \times 2$  supercells containing 33 and 129 atoms. There is no significant difference between the electronic stopping powers in this velocity range for the two supercell sizes, confirming that the  $2 \times 2 \times 2$  supercell is sufficient to produce accurate results.

A single k-point ( $\Gamma$ ) was used for the Brillouin zone integrations, after testing a ground state calculation with up to 90 k-points for convergence and simulation time. The difference between  $S_e$  for one k-point and 96, for trajectory number 1 and  $v = 1 \text{ a.u.}$ , was only  $0.2 \text{ eV/\AA}$ . A timestep of 1 attosecond was used for the low velocity simulations up to 1 a.u., and of 0.1 attoseconds for simulations above 1 a.u. after testing for the stability of the Crank-Nicolson integrator algorithm and the energy change in a TDDFT simulation. The plane-wave energy cutoff for real space integration was tested between 50 and 400 Ry; the total energy converged at around 150 Ry, and a 200 Ry cutoff energy was finally used in the simulations.

- <sup>1</sup> G. S. Was, *Fundamentals of Radiation Materials Science* (Springer-Verlag, 2007).
- <sup>2</sup> A. C. Begg, F. A. Stewart, and C. Vens, *Nat Rev Cancer* **11**, 239 (2011).
- <sup>3</sup> W. Käferböck, W. Rössler, V. Necas, P. Bauer, M. Peñalba, E. Zarate, and A. Arnau, *Phys. Rev. B* **55**, 13275 (1997).
- <sup>4</sup> S. D. Softky, *Phys. Rev.* **123**, 1685 (1961).
- <sup>5</sup> S. M. Seltzer and M. J. Berger, *The International Journal of Applied Radiation and Isotopes* **33**, 1189 (1982).
- <sup>6</sup> R. E. Newnham, *Properties of Materials* (Oxford, 2004).
- <sup>7</sup> O. H. Crawford, *Phys. Rev. A* **42**, 1390 (1990).
- <sup>8</sup> A. A. Shukri, F. Bruneval, and L. Reining, *Phys. Rev. B* **93**, 035128 (2016).
- <sup>9</sup> P. Echenique, R. Nieminen, and R. Ritchie, *Solid State Communications* **37**, 779 (1981).
- <sup>10</sup> P. M. Echenique, R. M. Nieminen, J. C. Ashley, and R. H. Ritchie, *Phys. Rev. A* **33**, 897 (1986).
- <sup>11</sup> T. L. Ferrell and R. H. Ritchie, *Phys. Rev. B* **16**, 115 (1977).
- <sup>12</sup> J. Lindhard, *Matematisk-fysiske Meddelelser* **28** (1954).
- <sup>13</sup> P. Echenique, F. Flores, and R. Ritchie, *Solid State Phys.* **43**, 229 (1990).
- <sup>14</sup> P. Sigmund, *Particle Penetration and Radiation Effects Volume 2* (Springer International Publishing, 2014).
- <sup>15</sup> D. R. Mason, J. le Page, C. P. Race, W. M. C. Foulkes, M. W. Finnis, and A. P. Sutton, *J. Phys. Condens. Matter* **19**, 436209 (2007).
- <sup>16</sup> C. P. Race, D. R. Mason, M. W. Finnis, W. M. C. Foulkes, A. P. Horsfield, and A. P. Sutton, *Rep. Prog. Phys.* **73**, 116501 (2010).
- <sup>17</sup> A. V. Krashennnikov, Y. Miyamoto, and D. Tománek, *Phys. Rev. Lett.* **99**, 016104 (2007).
- <sup>18</sup> J. M. Pruneda, D. Sánchez-Portal, A. Arnau, J. I. Juaristi, and E. Artacho, *Phys. Rev. Lett.* **99**, 235501 (2007).
- <sup>19</sup> M. A. Zeb, J. Kohanoff, D. Sánchez-Portal, A. Arnau, J. I. Juaristi, and E. Artacho, *Phys. Rev. Lett.* **108**, 225504 (2012).
- <sup>20</sup> A. A. Correa, J. Kohanoff, E. Artacho, D. Sánchez-Portal, and A. Caro, *Phys. Rev. Lett.* **108**, 213201 (2012).
- <sup>21</sup> M. A. Zeb, J. Kohanoff, D. Sánchez-Portal, and E. Artacho, *Nucl. Instrum. Meth. B* **303**, 59 (2013).
- <sup>22</sup> A. Ojanperä, A. V. Krashennnikov, and M. Puska, *Phys. Rev. B* **89**, 035120 (2014).
- <sup>23</sup> A. Caro, A. A. Correa, A. Tamm, G. D. Samolyuk, and G. M. Stocks, *Phys. Rev. B* **92**, 144309 (2015).
- <sup>24</sup> A. Schleife, Y. Kanai, and A. A. Correa, *Phys. Rev. B* **91**, 014306 (2015).
- <sup>25</sup> R. Ullah, F. Corsetti, D. Sánchez-Portal, and E. Artacho, *Phys. Rev. B* **91**, 125203 (2015).
- <sup>26</sup> M. Caro, A. A. Correa, E. Artacho, and A. Caro, *Sci. Rep.* **7**, 2045 (2017).
- <sup>27</sup> D. D. L. Chung, *J. Mater. Sci.* **37**, 1475 (2002).
- <sup>28</sup> J. Cazaux, *Solid State Commun.* **8**, 545 (1970).
- <sup>29</sup> E. Yagi, T. Iwata, T. Urai, and K. Ogiwara, *J. of Nucl. Mater.* **334**, 9 (2004).
- <sup>30</sup> A. Tsolakidis, D. Sánchez-Portal, and R. M. Martin, *Phys. Rev. B* **66**, 235416 (2002).
- <sup>31</sup> R. Ullah, A. Garaizar, F. Corsetti, J. Kohanoff, D. Sánchez-Portal, and E. Artacho, , forthcoming (2019).
- <sup>32</sup> J. M. Soler, E. Artacho, J. D. Gale, A. García, J. Junquera, P. Ordejón, and D. Sánchez-Portal, *J. Phys. Condens.*

- Matter **14**, 2745 (2002).
- <sup>33</sup> E. Artacho, E. Anglada, O. Diguez, J. D. Gale, A. Garca, J. Junquera, R. M. Martin, P. Ordejón, J. M. Pruneda, D. Sánchez-Portal, and J. M. Soler, *J. Phys. Condens. Matter* **20**, 064208 (2008).
- <sup>34</sup> S. Froyen, N. J. Troullier, J. L. Martins, L. C. Balbás, J. M. Soler, and A. Garcia, “ATOM, a program for DFT calculations in atoms and pseudopotential generation,” <https://departments.icmab.es/leem/siesta/Pseudopotentials/Code/downloads.html>.
- <sup>35</sup> N. Troullier and J. L. Martins, *Phys. Rev. B* **43**, 1993 (1991).
- <sup>36</sup> R. Ullah, E. Artacho, and A. A. Correa, *Phys. Rev. Lett.* **121**, 116401 (2018).
- <sup>37</sup> D. M. Ceperley and B. J. Alder, *Phys. Rev. Lett.* **45**, 566 (1980).
- <sup>38</sup> J. P. Perdew and A. Zunger, *Phys. Rev. B* **23**, 5048 (1981).
- <sup>39</sup> W. Kohn and L. J. Sham, *Phys. Rev.* **140**, A1133 (1965).
- <sup>40</sup> E. Runge and E. K. U. Gross, *Phys. Rev. Lett.* **52**, 997 (1984).
- <sup>41</sup> W. Pietsch, U. Hauser, and W. Neuwirth, *Nucl. Instrum. Methods* **132**, 79 (1976).
- <sup>42</sup> J. K. Tomfohr and O. F. Sankey, *Phys. Status Solidi B* **226**, 115.
- <sup>43</sup> E. Artacho and D. D. O’Regan, *Phys. Rev. B* **95**, 115155 (2017).
- <sup>44</sup> J. Deasy, *Med. Phys.* **21**, 709 (1994).
- <sup>45</sup> N.-P. Wang, I. Nagy, and P. M. Echenique, *Phys. Rev. B* **58**, 2357 (1998).
- <sup>46</sup> N.-P. Wang and I. Nagy, *Phys. Rev. A* **56**, 4795 (1997).
- <sup>47</sup> H. Winter, J. I. Juaristi, I. Nagy, A. Arnau, and P. M. Echenique, *Phys. Rev. B* **67**, 245401 (2003).
- <sup>48</sup> J. Lindhard, *Matematisk-fysiske Meddelelser* **14** (1965).
- <sup>49</sup> B. S. Elman, G. Braunstein, M. S. Dresselhaus, G. Dresselhaus, T. Venkatesan, and B. Wilkens, *J. Appl. Phys.* **56**, 2114 (1984).
- <sup>50</sup> T. Iwata, K.-I. Komaki, H. Tomimitsu, K. Kawatsura, K. Ozawa, and K. Doi, *Radiation Effects* **24**, 63 (1975).
- <sup>51</sup> D. Schroyen, M. Bruggeman, I. Dezi, and G. Langouche, *Nucl. Instrum. Meth. B* **15**, 341 (1986).
- <sup>52</sup> E. A. Figueroa, E. D. Cantero, J. C. Eckardt, G. H. Lantschner, J. E. Valdés, and N. R. Arista, *Phys. Rev. A* **75**, 010901 (2007).
- <sup>53</sup> S. N. Markin, D. Primetzhofer, S. Prusa, M. Brunmayr, G. Kowarik, F. Aumayr, and P. Bauer, *Phys. Rev. B* **78**, 195122 (2008).
- <sup>54</sup> D. Primetzhofer, S. Rund, D. Roth, D. Goebel, and P. Bauer, *Phys. Rev. Lett.* **107**, 163201 (2011).
- <sup>55</sup> S. N. Markin, D. Primetzhofer, M. Spitz, and P. Bauer, *Phys. Rev. B* **80**, 205105 (2009).
- <sup>56</sup> J. Junquera, O. Paz, D. Sánchez-Portal, and E. Artacho, *Phys. Rev. B* **64**, 235111 (2001).